PRAMANA
— journal of
physics

Vol. 76, No. 2
February 2011
pp. 271–279

Synchrotron radiation X-ray microfluorescence techniques and biological applications

R T LOPES[1,*], I LIMA[1,2], G R PEREIRA[1] and C A PEREZ[3]
[1]Nuclear Instrumentation Laboratory (LIN), COPPE, UFRJ, 21941-972 Rio de Janeiro, Brazil
[2]Department of Mechanical Engineering and Energy, Rio de Janeiro State University, Nova Friburgo, Brazil
[3]Brazilian Synchrotron Light Laboratory (LNLS), Campinas, Brazil
*Corresponding author. E-mail: ricardo@lin.ufrj.br

Abstract. Synchrotron X-ray imaging systems with fluorescence techniques was developed for biomedical researches in Brazilian Synchrotron Laboratory. An X-ray fluorescence microtomography system was implemented to analyse human prostate and breast samples and an X-ray microfluorescence system was implemented to study bone sites of human and animal samples with and without bone disorders.

Keywords. Synchrotron; X-ray; fluorescence; breast; bone.

PACS Nos 87; 87.59.-e; 87.64.kv

1. Introduction

The importance of some diseases worldwide, like cancer and osteoporosis, is very significant to the study of biological samples. The increase of mortality rate in Brazil due to cancer was a decisive factor in the choice of the investigated samples. The choice also reflects the scientists' wish to find diagnostic techniques for cancer and other diseases. The fluorescence mapping of iron, copper and zinc can be very important in diagnostics, because the biochemistry of these elements suggests that these metals may play important roles in carcinogenesis. But, the evidence linking iron, copper and zinc to cancer is far from conclusive and further research is needed [1]. Using X-ray fluorescence tomography the elemental map can be obtained without sample preparation.

Bone is a type of connective tissue and it consists essentially of protein and hydroxyapatite. These components can be distributed in different patterns in different types of bones. Mineral contents are correlated with mechanical properties contributing to bone strength [2]. Trace elements are found in both mineral and organic phases, although their role in normal bone function and in bone pathology is not fully established. The most famous and common bone illness is osteoporosis. It is a condition characterized by the

loss of bone density resulting in bones becoming more fragile and susceptible to fractures [3]. In this context, the knowledge of the distribution of major and trace elements is very significant to elucidate some important questions that remain unanswered or are controversial.

The X-ray fluorescence analysis is a microanalysis technique with extensive application in several fields of research and can supply important information about the sample's chemical properties to characterize samples with and without disorders [4–6]. In this work, X-ray fluorescence (XRF) techniques are used to analyse biological samples (prostate, breast and bone). The study used the XRF facility (D09B-XRF) at the Brazilian Synchrotron Light Laboratory (LNLS), Campinas, Brazil.

2. X-ray microfluorescence

Among X-ray microprobe methods based on synchrotron radiation, X-ray microfluorescence (μXRF) is an important method. This technique has been used successfully in academic circles in several applications, such as material, archeological and biological sciences. When a capillary optics is used, a good spatial resolution can be achieved ($\sim$1 μm). In this case, the beam suffers single or several reflections at the inner wall of the glass.

This analytical technique provides information about the chemical composition. When the X-ray impinges on the sample it interacts via photoelectric effect with the surface of the material which emits radiation that is characteristic of the atoms present in the sample. This emitted radiation is called X-ray fluorescent radiation and it is specific for each material. The fluorescent X-rays emitted by the material are collected by a solid-state detector and when associated with a multichannel analyser it produces a spectrum that involves the X-ray characteristic intensity (number of counts per second) of each chemical element and its energy. When X-ray fluorescence is associated with a synchrotron radiation (SR) source, many advantages, such as high energy, tunability and polarization of the X-rays can be achieved with respect to the usual X-ray source.

3. X-ray fluorescence microtomography

X-ray fluorescence microtomography (XRFμCT) is based on detection of photons from the fluorescent emission from the elements present in the sample. These photons are acquired by an energy dispersive detector, placed 90° to the incident beam direction. At each projection angle the line integral of the fluorescence along the beam inside the sample is measured. The sample is translated and another value is measured in the projection. These steps are repeated until the whole sample passes through the beam, completing the projection. The sample is rotated and another projection is measured. The projections are measured until the sample is rotated 180° [7].

The data acquisition of the XRFμCT results in a bi-dimensional raw data called sinogram. A sinogram consists of the line scans that are taken for every rotational angle. For each emission line of the fluorescence spectrum there is a separate sinogram. In general, a sinogram plots the property measured by the set-up over the direction perpendicular to the

beam and the angle of rotation. The tomogram which is a two-dimensional slice across the sample can be reconstructed from the sinogram by an appropriate algorithm.

4. Experimental conditions

This section presents the development of two different systems to study biological samples at the XRF facility (D09B-XRF) at LNLS.

4.1 *μXRFSR mapping*

Bone sites from human and animal samples with and without bone disorders were analysed. Femora and vertebrae of ∼300 μm of thickness were cut with a precision diamond saw and carefully placed in the experimental set-up to perform the bi-dimensional mapping. The amounts of P and Ca were mapped leading to an overall acquisition time of 4.5 h (10 s/step). The platform where the samples were placed can move in all the three directions (x, y and z). It has delimited the ROI and automated raster scans were performed.

The measurements were taken at LNLS, Campinas, Brazil. Currently, this facility has eleven beamlines. This experiment was carried out in the XRF beamline. The SR source

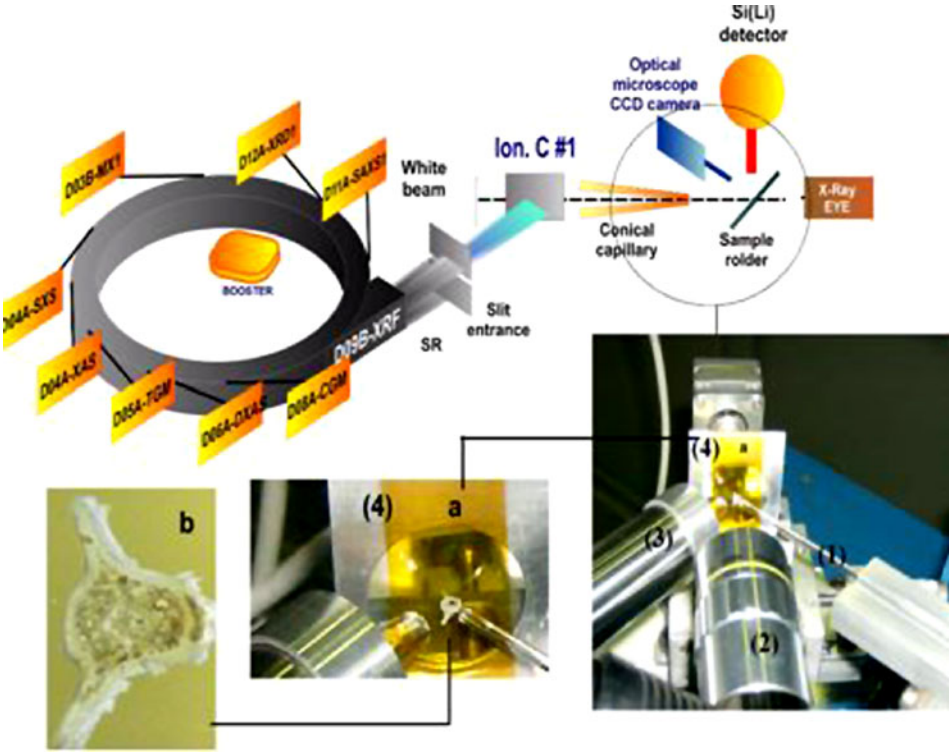

Figure 1. Experimental set-up of μXRFSR: (1) capillary optics, (2) microscope, (3) detector, (4) **a**: sample support, **b**: photograph of an animal vertebrae sample.

for the XRF beamline is at the D09B bending-magnet of the LNLS storage ring. For these measurements this line was equipped with an HPGe detector with a resolution of 150 eV at 5.9 keV. To excite the samples, a white beam was used and the sample holder was placed at 45° with respect to the detector and the incident beam. The beam was focussed by a fine conical capillary optics providing X-ray microbeam of 20 μm diameter. A microscope could be used to help the choice of the region of interest (ROI). Figure 1 shows this experimental set-up.

4.2 *XRFμCT*

XRFμCT was performed on human prostate and breast tissue samples. The component tissues were identified by the pathologist. The tissues were cut cylindrically with 1.5–2.0 mm thickness, 4.0–5.0 mm height, and were frozen and dried before being analysed.

A quasi-monochromatic beam produced by a multilayer monochromator at 12 keV, $\Delta E/E = 0.03$ collimated to a 200×200 μm^2 area with a set of slits, was used for sample excitation. The crystal monochromator was made of W-C with 75 layer pairs [8]. The intensity of the incident beam was monitored with an ionization chamber placed in front of it. A schematic of the experimental set-up for an X-ray fluorescence microtomography using a monochromatic beam is shown in figure 2.

The sample was placed on a high precision goniometer and translation stages that allow rotating as well as translating it perpendicularly to the beam. The fluorescence photons

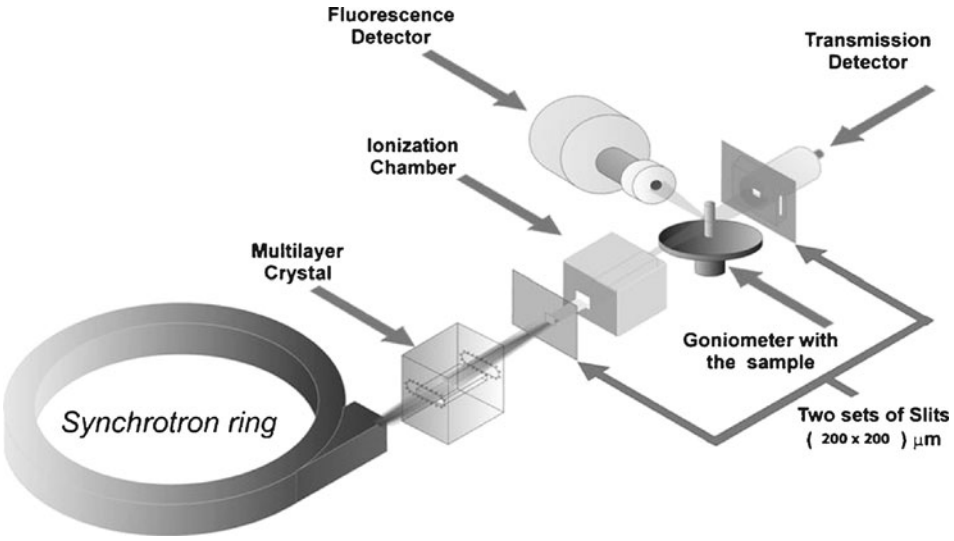

Figure 2. The experimental arrangement for an X-ray fluorescence microtomography measurement using a multilayer monochromator beam.

were collected with an energy-dispersive HPGe detector (CANBERRA Industries inc.) placed 90° to the incident beam, while transmitted photons were detected with a fast NaI (Tl) scintillation counter (CYBERSTAR-Oxford anfysik) placed behind the sample on the beam direction. This detector geometry reduces the elastic and Compton X-ray scattering from the sample due to the high linear polarization of the incoming beam in the plane of the storage ring, thus improving the signal-to-background ratio for the detection of trace elements [9].

The quality of the reconstruction is a compromise between the measuring time required for an acceptable counting statistics of the X-ray fluorescence peaks and the step size necessary to linearly move and rotate the samples. In one projection, samples were positioned in steps of 200 μm (actual beam size) perpendicular to the beam direction covering the whole transversal section of the sample proof. Each single value in a projection was obtained by measuring the fluorescence radiation emitted by all pixels along the beam. The object was then rotated, and another projection was measured. Projections were obtained in steps of 3° until the object completed 180°. The selected measuring time was 2 s for each scanned point.

The X-ray transmission and the X-ray fluorescence images were reconstructed using an in-house program developed using MATLAB® applying filtered-back projection algorithm. The absorption corrected matrix was obtained using MKCORR, a program developed by Brunetti and Golosio [10]. The 3D images were reconstructed using the 3D-DOCTOR software.

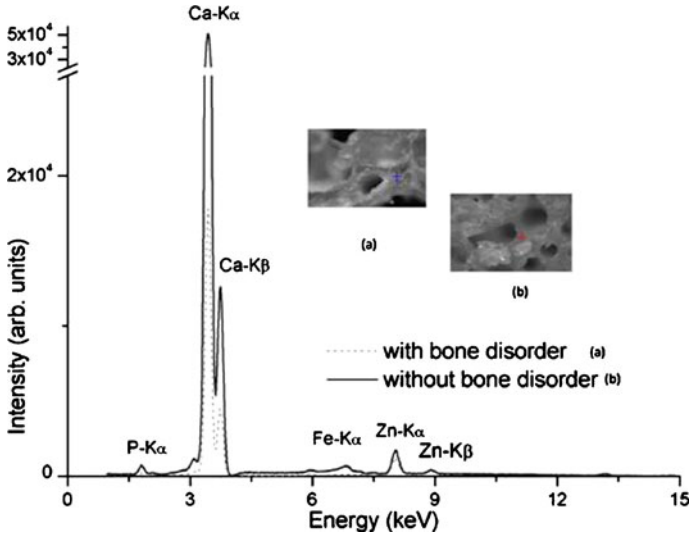

Figure 3. Typical SRμXRF spectrum for a bone sample with and without bone disorder.

5. Results and discussion

5.1 *μXRFSR mapping*

Figure 3 shows the typical SRμXRF spectrum for a bone sample with and without bone disorder. The cross in the figures shows the points where the measurements were

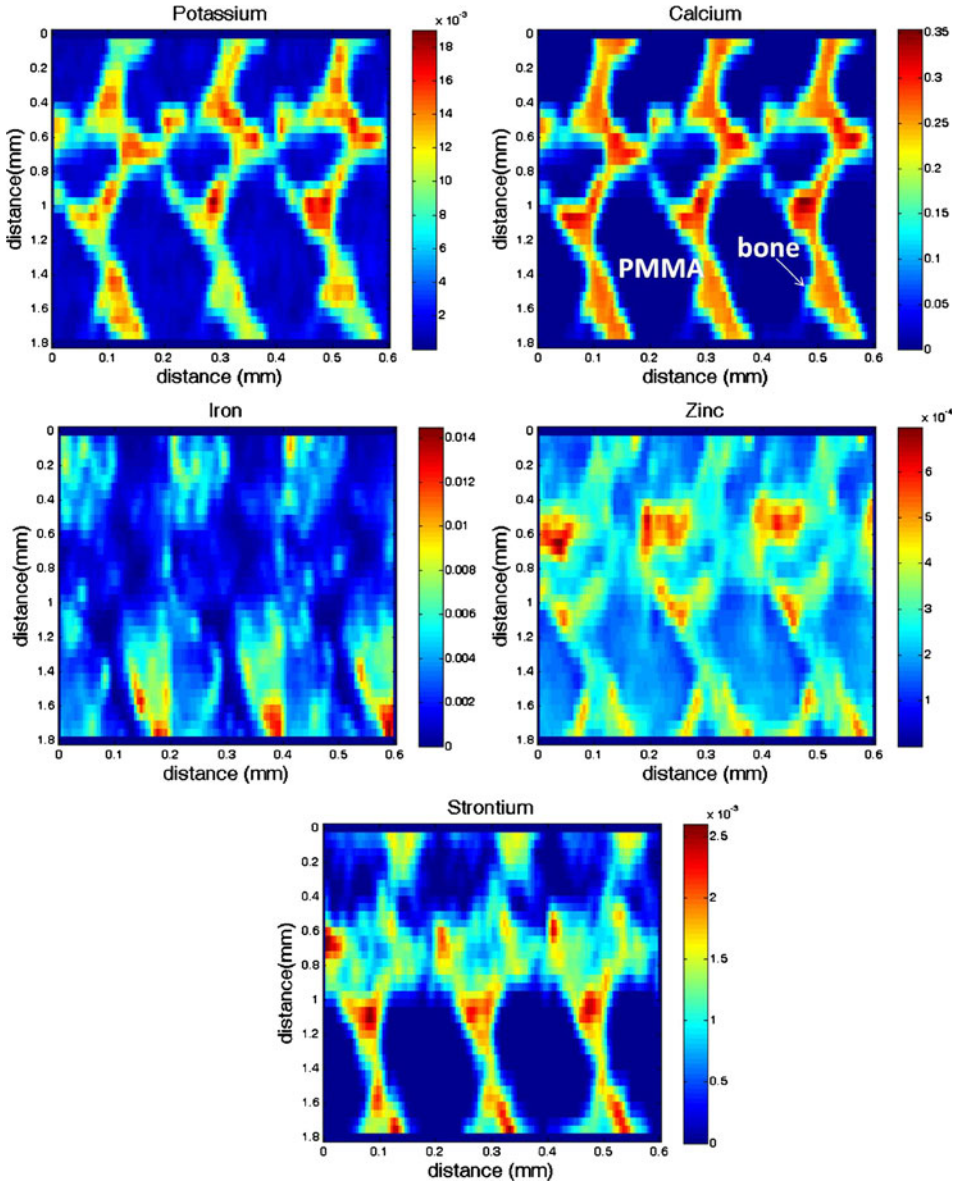

Figure 4. SRμXRF 2D map of a human biopsy embedded in PMMA.

performed (trabecular part of the bone). It is possible to identify P, Ca, Fe and Zn elements. The intensities of the elements in the sample without bone disorder are higher than those found in samples with bone disorder.

Figure 4 shows SRμXRF 2D map of a human biopsy embedded in polymethylmethacrylate (PMMA). It is possible to observe that P and Ca have similar distribution behaviour which is more localized inside the trabecular bone. Strontium and zinc seem to have the same trend, but much more heterogeneous. It is also possible to observe the presence of iron but not in the ring structure; it occurs on the periphery of the trabecular region. The PMMA does not influence chemical bone behaviour and it is clearly observed separately from bone.

Figure 5 shows P and Ca SRμXRF 2D map of an animal vertebra with and without bone disease. It is well known that bones consist essentially of a protein and hydroxyapatite in which the main minerals are P and Ca ($Ca_{10}(PO_4)_6(OH)_2$). Those images were taken at the lumbar vertebral body of Wistar rat which are trabecular regions with dimensions smaller than those found in human femora, as can be seen in figure 4. Similar behaviour

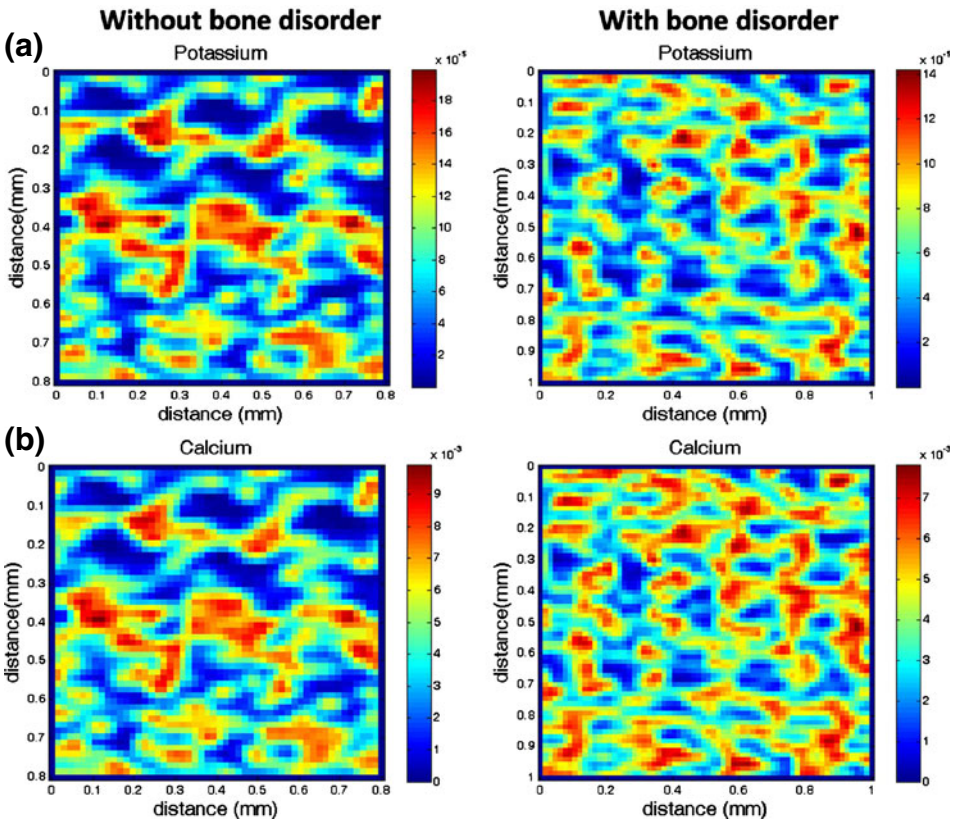

Figure 5. SRμXRF 2D map of an animal vertebra with and without bone disease.

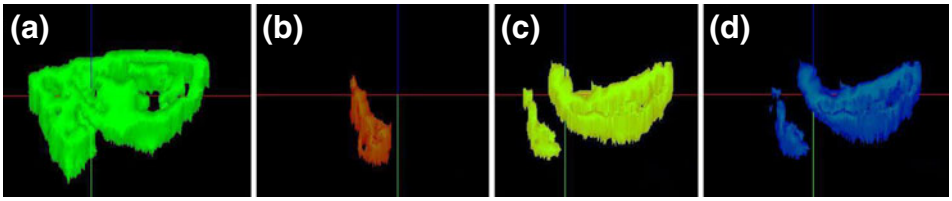

Figure 6. 3D tomographic images of a healthy breast sample: (**a**) μCT, (**b**) XRFμCT of iron, (**c**) XRFμCT of copper and (**d**) XRFμCT of zinc.

between the distribution of P and Ca was also found. In this case, P and Ca SRμXRF 2D map show that trabecular region of bone disorder is less organized than the one with lower mineral content.

5.2 *XRFμCT*

X-ray fluorescence microtomographies were performed on healthy human breast tissue samples and its results are shown in figure 6. It can be observed that the distribution of iron, copper and zinc in the healthy breast tissue is different and heterogeneous. There are some regions with no concentration of these metals. It can be seen in figure 6b that there is no iron in the entire sample except in a small part of that sample. Analysis of healthy and cancer breast samples led us to the discovery that the concentration of Fe is bigger in the tumour compared to healthy breast tissues of the same patient.

Figure 7 shows the 3D images of a prostate sample with benign prostatic hyperplasia (BPH). It was not possible to reconstruct the 3D XRFCT of copper because the concentration of this element in that sample was very small (less than 3 μg/g). Analysis of the prostate samples led to the discovery of the elemental distribution of iron, copper and zinc. It was verified that these tissues had a smaller concentration of copper and iron than zinc and the mean concentration of zinc in the BPH samples was about 150–300 μg/g.

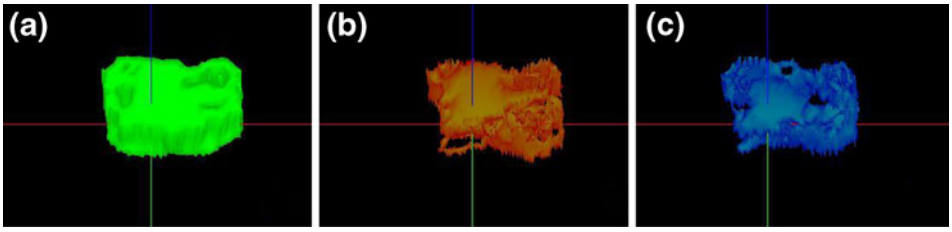

Figure 7. 3D tomographic images of a prostate sample with benign prostatic hyperplasia (BPH): (**a**) CT, (**b**) XRFμCT of iron, (**c**) XRFCT of zinc.

6. Conclusions

SRμXRF 2D map was demonstrated to be a powerful tool to study the bone mineral content and distribution showing the presence of other elements in addition to Ca and P. It was observed that trabecular regions with bone disorder have more disorganized structure than those regions without bone disorder. Analysing 3D images, it was observed that the distribution of iron, copper and zinc were different and heterogeneous in those samples. XRFCT technique enabled us to determine the elemental distribution of the elements inside the sample without destructing it. It is a useful tool in qualitative and quantitative analyses of biological tissues. The advantage of this technique is the three-dimensional visualization of the elemental distribution without material damages.

Acknowledgements

This work was partially supported by Conselho Nacional de Desenvolvimento Científico e Tecnológico (CNPq), Fundação de Amparo à Pesquisa do Estado do Rio de Janeiro (FAPERJ) and Laboratório Nacional de Luz Síncrotron (LNLS), projects: D09B-XRF–7049, 7079, 7715, 8056.

References

[1] H S Rocha, G R Pereira *et al*, *X-Ray Spectrom.* **36**, 247 (2007)
[2] J Rhoa, L Kuhn-Spearingb and P Ziouposc, *Med. Eng. Phys.* **20**, 92 (1998)
[3] S Wagner, A Stäbler, H Sittek, H Bonel, G Laeverenz, M F Reiser and A Baur-Melnyc, *Osteoporos. Int.* **16**, 1815 (2005)
[4] F W Bonner, L J King and D V Parke, *Chem. Biol. Interact.* **29**, 369 (1980)
[5] I Lima, M J Anjos, M L Fleiuss, D Rosenthal and R T Lopes, *X-Ray Spectrom.* **37**, 249 (2008)
[6] G R Pereira, H S Rocha *et al*, *Appl. Radiat. Isotopes* **68**(**4–5**), 704 (2010)
[7] G R Pereira, H S Rocha *et al*, *IEEE Trans. Nucl. Sci.* **56**, 1426 (2009)
[8] G R Pereira, H S Rocha *et al*, *X-Ray Spectrom.* **38**, 244 (2009)
[9] M Naghedolfeizi, J-S Chung *et al*, *J. Nucl. Mater.* **312**, 146 (2003)
[10] A Brunetti and B Golosio, *Comput. Phys. Commun.* **141**, 412 (2001)